A framework for coupled hydro-mechanical continuous modeling of gap-graded granular soils subjected to suffusion

Zhen-Yu YIN[1], Jie YANG[1, *], Farid LAOUAFA[2], Pierre-Yves HICHER[3]

Affiliations:

[1] Department of Civil and Environmental Engineering, The Hong Kong Polytechnic University, Hung Hom, Kowloon, Hong Kong, China

[2] National Institute for Industrial Environment and Risks (INERIS), Verneuil en Halatte, France

[3] Research Institute of Civil Engineering and Mechanics (GeM), UMR CNRS 6183, Ecole Centrale de Nantes, France

*Corresponding author: Dr. Jie YANG, Tel: +852 3400 8470; Fax: +852 2334 6389; Email: doc.jie.yang@gmail.com

Abstract: In order to study the impact of internal erosion at the scale of an engineering structure, a hydro-mechanical continuous modeling approach considering suffusion is needed. It requires a relevant mechanical model for granular soils considering the f_c-dependency (f_c: fines content) and a hydraulic model for suffusion to control the changes in the fines content. To this purpose, the mechanical models for granular soil, the unified modelling approaches for f_c-dependency of granular soils and the hydraulic modeling of suffusion are first reviewed. Then, a hydro-mechanical model considering both suffusion and mechanical loading is developed by combining the three components. For each component of the model, alternative choices are provided. Simulations of laboratory tests as well as an example of a dike-on-foundation problem demonstrated the reliability and applicability of this coupled numerical approach for internal erosion problems.

Keywords: granular soil, internal erosion, critical state, hydromechanical coupling, fines content

1. Introduction

Internal erosion occurs when fine particles are plucked off by hydraulic forces and transported through a coarse porous matrix. The known causes are either a concentration of leak erosion, backward erosion, soil contact erosion, or suffusion (Bonelli and Marot 2008; Fell et al. 2003; Wan and Fell 2004). This paper focuses on suffusion, which corresponds to the detachment

and migration of fine particles within the voids between the coarse particles due to seepage flow.

From an engineering point of view (Kenney and Lau 1985), the granular material is composed of a primary particle fabric and loose particles. The primary particle fabric supports the loading forces. Within the pores of the primary fabric, there are loose and erodible fine particles which can be displaced by water flow. Any change of the soil microstructure induced by the loss of fine particles may also modify the soil behavior and induce deformations at the macroscopic scale. Internal erosion can be the cause of many damages, failures or collapses of embankment dams (Fell et al. 2003; Rönnqvist et al. 2014; Xu and Zhang 2009; Zhang and Chen 2006; Zhang et al. 2009). Besides, internal erosion can also trigger sinkholes and cavities, as it has frequently been observed within dams and dikes (Muir Wood 2007; Sterpi 2003), as well as slope failure or instability and significant landslides (Crosta and Prisco 1999; Hu et al. 2018).

Different numerical approaches have been developed to describe the erosion process, either within the framework of continuum mechanics using the finite element or finite difference methods (Cividini and Gioda 2004; Papamichos et al. 2001; Stavropoulou et al. 1998; Vardoulakis et al. 1996; Yang et al. 2019a; Yang et al. 2019c, 2019d, 2019e; Zhang et al. 2013) or within a discrete framework by coupling the discrete element method to describe the dynamics of the granular solid phase to the fluid dynamics to solve the interstitial fluid flow (Lominé et al. 2013; Mansouri et al. 2017; Reboul et al. 2008; Sari et al. 2011; Sibille et al. 2015; Zhang et al. 2018; Zhao and Shan 2013). These studies focused mainly on the hydraulic process, i.e. the evolution of the eroded mass and permeability. The mechanical part was simplified through an elastic model with damage parameters. Some attempts have been made to model the mechanical response to internal erosion by removing particles in granular materials (Hicher 2013; Hosn et al. 2018; Muir Wood et al. 2010; Scholtès et al. 2010). However, the removal was based on the size of the particles or the level of interlocking, and the real process of erosion was not considered.

Even though the discrete element method has proved its efficiency in explaining the mechanical properties of granular materials, its prohibitive computational cost becomes an obstacle whenever real soil structures such as embankment dams are analyzed. Hence, it is necessary to develop an approach more suitable for engineering boundary value problems at a real space scale to provide the hydro-mechanical response of soils subjected to internal erosion.

Vardoulakis et al. (1996) developed a mathematical model for sand production in boreholes. Piping and surface erosion effects were studied based on the mass balance and particle transport equations, as well as on the fluid flow in a porous continuous medium described by Darcy's law. The derived governing equations were solved numerically using the finite difference method in 1D condition. This model was then enhanced by Stavropoulou et al. (1998) by taking into account the mechanical damage induced by sand erosion. The mathematical model was solved numerically by using the finite element method. Similar mathematical models have been developed by Papamichos et al. (2001), Cividini and Gioda (2004), Steeb et al. (2007), Uzuoka et al. (2012), Zhang et al. (2013). However, none of these models could accurately take into account the modification in the soil shear strength during and after internal erosion. The mechanical part consisting of an elastic model with damage remained too simple for this purpose.

To solve the engineering problem, a coupled hydro-mechanical continuous modeling approach considering suffusion is needed. It requires (a) an advanced but relatively simple mechanical model for granular soils, (b) a mechanical modeling considering the f_c-dependency of granular soils due to fines eroded or infiltrated, (c) a hydraulic modeling of suffusion to describe how the fines content changes. The paper presents a review on these three key components. A hydro-mechanical model considering both suffusion and mechanical loading could be developed by combining the three components. For each component of the model (mechanical model, f_c-dependency and erosion law), alternative choices can be made.

2. A suitable mechanical constitutive model for granular soils

Numerous constitutive models have been developed in order to describe the complex behaviors of granular soils. These models can be classified as (1) nonlinear hypoelastic models (Duncan and Chang 1970), (2) incrementally nonlinear model (Darve 1990; Darve and Labanieh 1982), (3) hypoplastic models (Mašín and Khalili 2012; Niemunis and Herle 1997; Wu et al. 1996), (4) elastoplastic models (Gajo and Wood 1999; Jefferies 1993; Jin et al. 2016; Taiebat and Dafalias 2008; Vermeer 1978; Yao et al. 2004; Yao et al. 2008; Yu 1998), and (5) micromechanics-based models (Chang and Hicher 2005; Chang and Yin 2009; Nicot and Darve 2011; Wan and Pouragha 2015; Yin et al. 2010; Yin et al. 2014). In general, the first four categories are phenomenological models, which are commonly adopted in engineering practice due to their efficiency in finite element analyses.

According to the mechanical behaviors of granular materials, a phenomenological model should be able to describe the frictional behaviors (asymptotic relationship between the stress ratio and the shear strain), the contractive or dilative behaviors (shear-induced volume change), the critical state behaviors (the unique ultimate state of a given material attainable in the *p*-*q* and *e*-*p* planes for any initial state). The critical state based models are good choices (Table 1), since they can successfully capture all these mechanical features with more or less complicated formulations. Among the critical state based models, the SIMSAND model is a representative one (summarized in Table 2). It was chosen to be the basic model of the mechanical part in the following hydromechanical modelling of internal erosion.

Table 1 Summary of critical-state based models for granular soils

Model name	References
Nor-Sand model	(Jefferies 1993)
CSAM model	(Yu 1998)
Severn–Trent sand model	(Gajo and Wood 1999)
UH models	(Yao et al. 2014; Yao et al. 2004; Yao et al. 2008; Yao et al. 2009)
SANISAND model	(Taiebat and Dafalias 2008)
SIMSAND model	(Jin et al. 2016; Jin et al. 2017; Jin et al. 2018; Wu et al. 2017)
Hypoplasticity models	(Kolymbas 1991; Mašín 2005; Wu and Kolymbas 2000; Wu et al. 1996)
Exponential function based endochronic model	(Yin et al. 2018)
Modified stress-dilatancy model	(Wan and Guo 1998)

Table 2 Basic constitutive equations of SIMSAND

Components	Constitutive equations
Elasticity	$\delta\varepsilon_{ij}^{e}=\frac{\delta\sigma'}{2G_{ij}}-\frac{\upsilon\delta\sigma'_{kk}\delta_{ij}}{2G(1+\upsilon)}$ $G=G_0 p_{at}\frac{(2.97-e)^2}{(1+e)}\left(\frac{p'}{p_{at}}\right)^n, K=K_0 p_{at}\frac{(2.97-e)^2}{(1+e)}\left(\frac{p'}{p_{at}}\right)^n$
Yield surface in shear	$f_s=q/p'-H$
Potential surface in shear	$\frac{\partial g_s}{\partial p'}=A_d\left(M_{pt}-q/p'\right);\ \frac{\partial g_s}{\partial s_{ij}}=\{1\ \ 1\ \ 1\ \ 1\ \ 1\ \ 1\}$
Hardening rule for shear	$H=M_p\varepsilon_d^p\Big/\left(k_p+\varepsilon_d^p\right)$
Critical state line and inter-locking effect	$e_c=e_{cr0}-\lambda\left(p'/p_{at}\right)^{\zeta},\ \tan\varphi_p=\left(e_c/e\right)^{n_p}\tan\varphi_\mu,\ \tan\varphi_{pt}=\left(e/e_c\right)^{n_d}\tan\varphi_\mu$ $M_p=6\sin\phi_p\Big/\left(3-\sin\phi_p\right),\ M_{pt}=6\sin\phi_{pt}/3-\sin\phi_{pt}$

* p_{at} is the atmospheric pressure (p_{at} = 101.325 kPa); p' is the mean effective stress; q is the deviatoric stress; ϕ_p is peak fiction angle; ϕ_{pt} is phase transformation friction angle; M_p and M_{pt} is the stress ratio corresponding to peak strength and phase transformation strength respectively; e_c is the critical void ratio;

* Parameters: G_0 and K_0 the dimensionless referential shear and bulk modulus; ν the Poisson's ratio; n the elastic constant controlling nonlinear stiffness; k_p the plastic shear modulus; A_d the stress-dilatancy parameter; ϕ_μ is critical fiction angle; n_p and n_d the constants controlling the nonlinearity of inter-locking effect; λ and ζ the constants controlling the slope and nonlinearity of CSL in the e–log p' plane; e_{cr0} is the reference critical void ratio corresponding to $p_{ref}=p_{at}$;

The drained and undrained triaxial tests performed by Miura et al. (1984) on Toyoura sand with different initial void ratios were selected to examine the performances of the SIMSAND

model. One isotropic compression test and three drained triaxial tests were used to calibrated the model parameters (see (Wu et al. 2019)). The determined parameters (summarized in Table 3) are used to simulate another three drained and three undrained triaxial tests as presented in Figure 1. All the simulations generally in agreement with the experimental data, demonstrating that the SIMSAND model gives reasonable and reliable results to describe the mechanical behaviors of granular materials. Note that other models as summarized in Table 1 can also give good predictive performances on the mechanical response of sand.

Table 3 Parameters of SIMSAND

Elastic parameters			Plastic parameters			CSL-related parameters				
G_0	ν	n	k_p	A_d	ϕ_u	e_{cr0}	λ	ζ	n_p	n_d
78	0.25	0.52	0.0038	0.78	31.8	0. 937	0.039	0.365	3.49	2.65

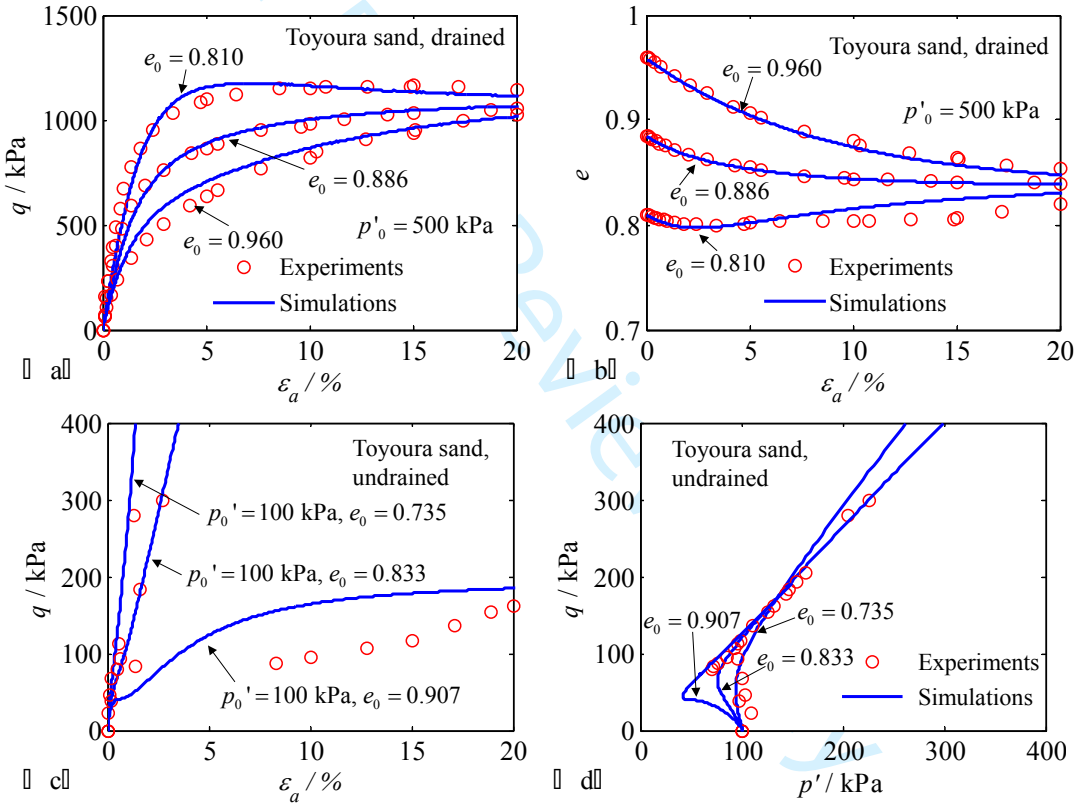

Figure 1 Comparison between experiments and simulations for drained (a-b) and undrained triaxial tests (c-d) on Toyoura sand: (a,c) deviatoric stress versus axial strain, (b) void ratio versus axial strain, (d) deviatoric stress versus mean effective stress

3. A unified modelling approach for f_c-dependency

3.1. Unified formulations for index void ratios of gap-graded granular soils

Natural soils or man-made fills are often mixtures of multi-size grains. The void ratio of a granular soil varies with the grain packing arrangement. Numerous analytical models have been developed to describe the density of grain packing. These models can be mainly classified as

(1) polynomial model (e.g., (Chang and Deng 2018; Yin et al. 2016; Yu and Standish 1987, 1988)): the specific volume of a packing mixture is a polynomial function of the volume fraction of each size class of particles. The filling mechanism (small particles are filled into the large-particle skeleton), the embedment mechanism (large particles are embedded into the small-particle matrix), the loosening effect (small particles filled into the large-particle skeleton push apart the surrounding large particles) and the wall effect (large particles embedded into the small-particle matrix create void spaces at the interface between the large particle and the surrounding small particles) can be reasonably represented. (2) Fractal model (e.g., (Liu et al. 2019; Liu et al. 2018; Minh and Cheng 2013)): the particle-size distribution of granular soils is considered fragmentally fractal and, accordingly, fractal dimensioning techniques have been used to quantify the size distribution of relatively well-graded granular soils.

Regarding the index void ratios of gap-graded granular soils (binary materials), the expression of the inter-grain contact index and its extension proposed by Yin et al. (2016) was clear and easy to be applied in practice. The void ratio of the soil mixture e introduced by Chang and Yin (2011) and Thevanayagam et al. (2002) can be unified by the fines content, as follows, by taking into account the transition zone from a coarse-grain to a fine-grain skeleton:

$$e=\left[e_{hc}\left(1-f_c\right)+af_c\right]\frac{1-\tanh\left[\xi\left(f_c-f_{th}\right)\right]}{2}+e_{hf}\left(f_c+\frac{1-f_c}{\left(R_d\right)^m}\right)\frac{1+\tanh\left[\xi\left(f_c-f_{th}\right)\right]}{2} \quad \text{.....(1)}$$

where f_c is the mass fraction of fine grains in the soil mixture; a is a material constant depending on the fabric structure of the soil mixture (e.g. grading, particle shape); R_d is the ratio of the mean size of coarse grains D_{50} to the mean size of fine grains d_{50}; m is a coefficient depending on grain characteristics and fine grain packing; e_{hc} and e_{hf} are the void ratios of coarse grains and fine grains; where ξ (=20, can be fixed) is a material constant controlling the evolution rate of the transition zone; f_{th} is the threshold fines content from a coarse grain to a fine grain skeleton; the hyperbolic tangent function is expressed as $\tanh x=\left(e^{2x}-1\right)/\left(e^{2x}+1\right)$ for ensuring a smooth transition zone. The validation of Eq.(1) was obtained by comparing $e_{\min}$ and $e_{\max}$ of soil mixtures for various sand-silt mixtures (Yin et al. 2016).

The overall void ratio index can also be obtained by other approaches mentioned above, such as the approach based on the hypothesis of a dominant size of packing mixtures by Chang and

Deng (2018), fractal analysis by Liu et al. (2019; 2018), a void space based theoretical model by Shen et al. (2019). Note that Eq.(1), even if its mathematical expression appears complicated, is easy to use in practice since its parameters can be easily obtained from standard tests.

3.2. Application to the location of the critical state line

According to the critical state theory, the void ratio, as well as its relationship with the mean effective stress, has a governing influence on the deformation and strength characteristics of granular soils. Similar to $e_{\min}$ and $e_{\max}$, the fines content was shown to influence significantly the location of the critical state line of granular mixtures in the *e-p'* plane. (Papadopoulou and Tika 2008; Thevanayagam et al. 2002; Yang et al. 2006; Zlatović and Ishihara 1995). According to Li and Wang (1998), the critical state line can be expressed as:

$$e_c = e_{cr0} - \lambda \left(\frac{p'}{p_{at}} \right)^{\varsigma} \quad \text{.....(2)}$$

where e_{cr0} is the reference critical void which determines the position of the CSL in the $e-p'$ plane. $p_{at} = 101.325\ kPa$ is the atmospheric pressure. λ and ς are material constants controlling the non-linearity of the critical state line.

Adopting the form of Eq.(1), the evolution of e_{cr0} with fines content can be determined as follows:

$$e_{cr0} = \left[e_{hc,cr0} \left(1 - f_c\right) + a f_c \right] \frac{1 - \tanh\left[\xi\left(f_c - f_{th}\right)\right]}{2} + e_{hf,cr0} \left(f_c + \frac{1 - f_c}{\left(R_d\right)^m} \right) \frac{1 + \tanh\left[\xi\left(f_c - f_{th}\right)\right]}{2} \quad \text{.(3)}$$

where $e_{hc,cr0}$ and $e_{hf,cr0}$ are the reference critical void ratios for coarse and fine grains, respectively. a, m, ξ and f_{th} are fines content related parameters: a controls the slope of the curve $e_{cr0} - f_c$ for the silty sand varying from -1.0 to 1.0; m controls the slope of the curve $e_{cr0} - f_c$ for the sandy silt varying from 0.0 to 1.0; ξ controls the evolution rate of the transition zone ($\xi = 20$, can be fixed), f_{th} is the threshold fines content from a coarse grain skeleton to a fine grain skeleton, varying usually from 0.2 to 0.35 on the basis of existing experimental data.

The location of the critical state line can, therefore, be obtained by combining Eqs.(2) and (3) for sand-silt mixtures with different fines contents. This expression can then be implemented

within a critical-state based constitutive model (e.g., the SIMSAND model shown in Table 2) with 5 additional parameters ($e_{hc,cr0}$, $e_{hf,cr0}$, a, m and f_{th})

3.3. Performance of the unified model

Undrained triaxial compression tests on isotropically consolidated samples of sand-silt mixtures by Thevanayagam et al. (2002) were selected and simulated by the f_c-dependent sand-silt mixture model (see Table 2 and Eqs.(2) and (3)). Soil mixtures (R_d=25) were prepared using Foundry sand as the host sand mixed with various amounts of non-plastic crushed silica fines (No.40) at 0,7,15,25,40,60 and 100% fines by dry weight. The initial void ratios and initial critical void ratios of selected tests were plotted in Figure 2. The elastic parameters (G_0, ν, n) and plastic parameters were calibrated using three undrained triaxial tests with f_c=0% (see (Yin et al. 2016)), the CSL-related parameters ($e_{hc,cr0}$, $e_{fc,cr0}$, λ, ζ) and fines content related parameters were calibrated by the CSL in e-logp' plan for various fines content with $n_p = n_d = 1$. The determined model parameters (summarized in Table 4) are used to simulate the undrained triaxial tests with different fines content.

Table 4 Values of model parameters for Foundry sand–silt mixtures

Elastic parameters			Plastic parameters			CSL-related parameters				Fines parameters		
G_0	ν	n	k_p	A_d	ϕ_d	$e_{hc,cr0}$	$e_{fc,cr0}$	λ	ζ	a	m	f_{th}
150	0.2	0.5	0.0033	1	30	0.795	0.86	0.03	0.68	-0.4	0.55	0.25

Figure 3 shows the comparison between the measured and the predicted results for the samples subjected to undrained triaxial tests. Under undrained condition, the decrease of fines content may lead to a static liquefaction. In the case of suffusion, the loss of fine particles affects the interlocking, i.e., the density state (e_0/e_c), by changing simultaneously the void ratio e and the critical void ratio e_c. The specimen could reach static liquefaction when $e_0/e_c>1$. The unified f_c-dependent model is capable of describing the mechanical characteristics of soils under suffusion by linking the soil's density state (e_0/e_c) with the change of fines content (f_c). More discussions could be found in Yang et al. (2019b) and Yang et al. (2019a). The results demonstrate that the model can reproduce, with relative success, both the effect of the fines on the silty sand behavior and the effect of the coarse grains on the sandy silt behavior. However, discrepancies were observed for samples subjected to static liquefaction. In that case, the model was able to obtain correctly the maximum deviatoric strength, but the stress- strain behavior after the peak was not well reproduced due to a more rapid decrease of the deviatoric stress in the simulation compared to the experimental data. In fact, it is very hard to prepare identical samples for sand with fines. Thus, in this case, comparing the trend of mechanical response

makes more sense than comparing absolute values. Besides, note that the fines and coarse grains were from the same origin, with similar morphological characteristics for fine and coarse grains. As a consequence, the critical friction angle was assumed to be independent of the fines content. Otherwise, a more complicated bi-material composite approach, such as a homogenization method using parallel modelling (or Voigt hypothesis) or series modelling (or Reuss hypothesis), would have had to be applied.

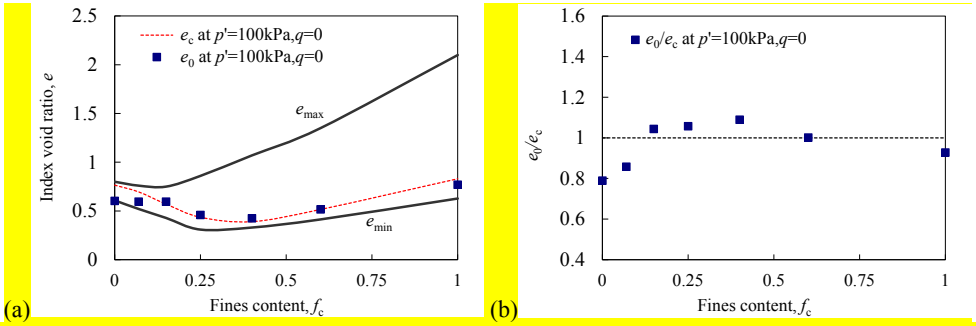

Figure 2 (a) Initial void ratios and initial critical void ratios and (b) initial density state (e_0/e_c) of selected tests

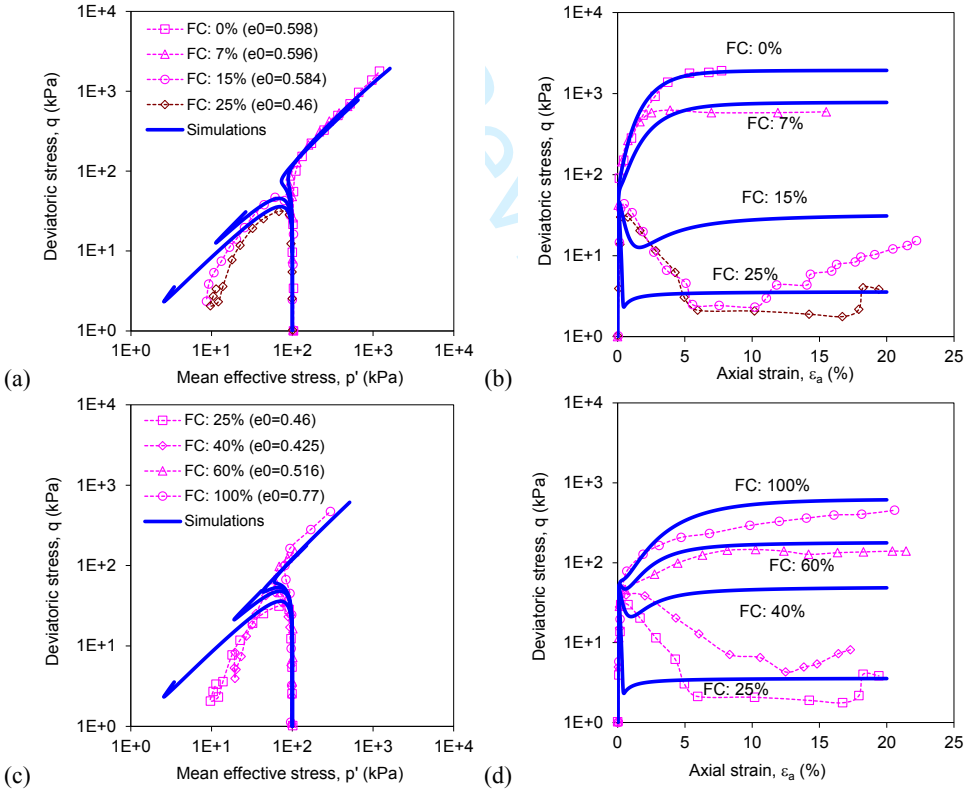

Figure 3 Comparison of experimental results and simulations for Foundry sand subjected to undrained triaxial tests, with fines content varying from 0 to 100%

4. Hydraulic modelling of suffusion

A numerical modelling approach has been formulated to describe the detachment, the transport, and the clogging of fine particles during suffusion. This approach treats the material as a

continuous medium. According to Schaufler et al. (2013), it is possible to consider the saturated porous medium as a material system composed of 4 constituents: the stable fabric of the solid skeleton (*ss*), the erodible fines (*se*), the fluidized particles (*fp*) and the pure fluid phase (*ff*), as shown in Figure 4. The fines can behave either as a fluid-like (described as fluidized particles) or as a solid-like (described as erodible fines) material. The detachment of the fine particles, i.e. the transformation of fine particles from solid-like fines to fluidized fines was described by the mass exchange between the solid and the fluid phases. Filtration could be incorporated into the mass exchange term to simulate the clogging. The transport of the fines particles was described by the mass balance of the 4-constituents system.

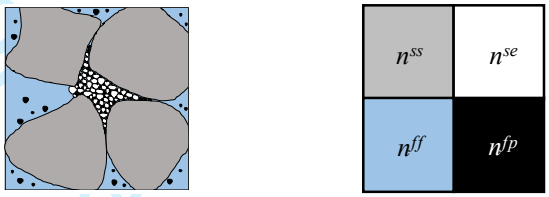

(a) Micro-scale (b) 4 constituents

Figure 4 REV of a fully-saturated soil mixture and the four-constituent continuum model

4.1. Mass balances and transported particles

The balance equations were derived based on the porous medium theory (de Boer 2000; Steeb and Diebels 2003; Uzuoka and Borja 2012). In a given Representative Elementary Volume (REV), the volume balance of a constituent is deduced from the partial balance of mass (Vardoulakis et al. 1996), given as:

$$\frac{\partial\left(n^i\right)}{\partial t}+\operatorname{div}\left(n^i\mathbf{v}^i\right)=n_i^{ex} \qquad -n_{fp}^{\mathrm{ex}}=n_{se}^{\mathrm{ex}}=\hat{n},\ n_{ss}^{\mathrm{ex}}=0,\ n_{ff}^{\mathrm{ex}}=0 \qquad \text{.....(4)}$$

with $i=\{ss,se,ff,fp\}$ denoting the 4 constituents, n_i, $\mathbf{v}_i$ and n_i^{ex} denoting, respectively, the volume fraction, the velocity and the volumetric mass exchange of the corresponding constituent. $\hat{n}$ is the volumetric mass exchange for transformation of fine particles from solid-like fines (*se*) to fluidized fines (*fp*).

A system of non-linear partial differential equations could be deduced from the mass balance of the mixture system:

$$-\frac{\partial\phi}{\partial t}+\operatorname{div}\left(\mathbf{v}_s\right)-\operatorname{div}\left(\phi\mathbf{v}_s\right)=\hat{n} \qquad \text{.....(5)}$$

$$\frac{\partial\left(f_c\right)}{\partial t}-\frac{\partial\left(f_c\phi\right)}{\partial t}+\operatorname{div}\left(f_c\mathbf{v}_s\right)-\operatorname{div}\left(f_c\phi\mathbf{v}_s\right)=\hat{n} \qquad \text{.....(6)}$$

$$\frac{\partial(c\phi)}{\partial t}+\mathrm{div}(c\mathbf{q}_{\mathbf{w}})+\frac{\partial(c\phi\mathbf{v}_s)}{\partial t}=-\hat{n} \quad \text{.....(7)}$$

$$\mathrm{div}(\mathbf{q}_w)+\mathrm{div}(\mathbf{v}_s)=0 \quad \text{.....(8)}$$

where $\phi(x,t)$, $f_c(x,t)$ and $c(x,t)$ are the porosity, the fraction of erodible fines and the concentration of the fluidized particles, respectively; $\mathbf{v}_s$ is the velocity of the soil skeleton with $\partial(\varepsilon_v)/\partial t=-\mathrm{div}(\mathbf{v}_s)$, ε_v is the volumetric strain; $\mathbf{q}_w(x,t)$ is the total discharge of the pore fluid. For the sake of legibility, the time t and the space $\mathbf{x}$ variables have been omitted in the equations.

Eq.(5) describes the evolution of the solid phase (solid skeleton and erodible fines). Eq.(6) represents the balance of volume of the erodible fines, whereas Eq.(7) is the balance of volume of the fluidized particles describing the production and transport of fluidized fine particles. The balance of the mass of the mixture, *i.e.*, the continuity equation, is given by Eq.(8). Note that the fraction of fines content f_c can be obtained explicitly from the current porosity ϕ and the volumetric strain ε_v, which indicates that Eq.(6) can be replaced by:

$$f_c=1-\frac{(1+\varepsilon_v)(1-\phi_0)(1-f_{c0})}{1-\phi} \quad \text{.....(9)}$$

where $\phi_0(x)$ and $f_{c0}(x)$ denote the initial value of $\phi(x,t)$ and $f_c(x,t)$, respectively.

4.2. Porous fluid flow

In this study, the flow in the porous medium was assumed to be governed by Darcy's law:

$$\mathbf{q}_{\mathbf{w}}=-\frac{k(f_c,\phi)}{\eta_k\bar{\rho}(c)}\mathbf{grad}(p_w) \quad \text{.....(10)}$$

where $p_w(x,t)$ is the pore fluid pressure; $k(f_c,\phi)$ is the intrinsic permeability of the medium; η_k is the kinematic viscosity of the fluid; $\bar{\rho}(c)$ is the density of the mixture defined as:

$$\bar{\rho}=c\rho_s+(1-c)\rho_f \quad \text{.....(11)}$$

with ρ_s and ρ_f denoting the density of the solid and the fluid. For a mixture, the intrinsic permeability $k(x,t)$ of the porous medium depends on the current porosity $\phi(x,t)$ and on the fines content as (Revil and Cathles 1999):

$$k=k_0\left[1-f_c(1-\phi)\right]^{3m_k} \quad \text{.....(12)}$$

where m_k is the so-called "cementation exponent" and varies with the pore geometry. A high value of the cementation exponent indicates a strong decoupling between the total interconnected porosity and the effective porosity that controls the flow.

4.3. Erosion law: coupling of erosion and filtration

Eqs.(5)-(12) could describe the evolution of ϕ, f_c, c and q_w, however, for a boundary value problem, the volumetric mass exchange term $\hat{n}$ needs to be defined. $\hat{n}$ corresponds to the rate of the eroded mass volume ($\hat{n}_e$) and the filtrated mass volume ($\hat{n}_f$) at any time and any point:

$$\hat{n} = \hat{n}_e + \hat{n}_f \quad \text{.....(13)}$$

Different expressions for the erosion law proposed in the literature are summarized in Table 5. Alternative choices for the erosion law can be made according to the analysis conditions.

Table 5 Summary of erosion laws for internal erosion problem

	Erosion law	Parameters	References
①	$\hat{n}_e = -\lambda_e(1-\phi)(f_c - f_{c\infty})\lvert\mathbf{q}_w\rvert$ $f_{c\infty} = f_{c0}\left[(1-\alpha_1)\exp\left(-\lvert\mathbf{q}_w\rvert\times 10^{\alpha_2}\right)+\alpha_1\right]$ $\hat{n}_f = \lambda_f \frac{\phi-\phi_{\min}}{\phi^{\beta}} c\lvert\mathbf{q}_w\rvert$	λ_e, λ_f : material parameters α_1, α_2 : material parameters controlling the ultimate fines content β : material parameters related to the heterogeneity of the soil mixture	(Uzuoka et al. 2012) (Cividini et al. 2009) (Yang et al. 2019e)
②	$\hat{n}_e = -\lambda_e \frac{(1-\phi)}{k} c\lvert\mathbf{q}_w\rvert$ $\hat{n}_f = \lambda_f \frac{(1-\phi)}{k}\frac{c^2}{c_{cr}}\lvert\mathbf{q}_w\rvert$	λ_e, λ_f : material parameters c_{cr} : critical value of c for which the erosion and deposition balance each other	(Vardoulakis et al. 1996)
③	$\hat{n}_e = -k_d\left((\Delta h/L)\sqrt{2k\eta\gamma_w/\phi} - \tau_c\right)$	k_d, τ_c : material parameters Δh : hydraulic head drop L : seepage length η : dynamic viscosity of the fluid	(Reddi et al. 2000)
④	$\hat{n}_e = -\lambda_e(1-\phi)c\mathbf{q}_w \cdot \mathbf{q}_w$	λ_e : material parameter	(Steeb et al. 2007)
⑤	$\hat{n}_f = \lambda_f c\lvert\mathbf{q}_w\rvert$	λ_f : material parameter	(Schaufler et al. 2013)
⑥	$\hat{n}_e = -\lambda_e f_c\lvert\mathbf{q}_w\rvert$	λ_e : material parameter	(Khalil et al. 2013)

4.4. Performance of the hydraulic model

The governing equations (5)-(8), coupled with the erosion-filtration law (Table 5), make up an unsteady, coupled non-linear system of partial differential equations. This system of partial differential equations could be solved through the classic difference procedure.

The erosion tests performed by Rochim et al. (2017) on gap-graded sand and gravel mixtures were selected to examine the model performance. Three gap-graded sand-gravel mixtures with different initial fines contents (20% for soil A, 25% for soil B and 29% for soil C) under two different hydraulic loadings were simulated (named 'a' and 'b'). The first multistage hydraulic

gradient condition (named 'a') consisted of increasing the hydraulic gradient by steps of 0.1, 0.15, 0.2 and 0.25 up to 0.5, 0.8, 1 and 2, respectively, then by steps of 0.5 between 2 and 4 and by steps of 1 beyond 4. For the second kind of hydraulic loading (named 'b'), the hydraulic gradient increment was directly imposed equal to 1. For both hydraulic loadings, each stage of the hydraulic gradient was kept constant for 10 min. Erosion law ① (in Table 5) was adopted where 5 model parameters are needed (λ_e, λ_f, α_1, α_2, β). 1 parameter (m_k) is needed for permeability. The initial dry density for soil mixture A, B and C are 17.39, 18.74 and 18.74 kN/m^3 respectively. C97-a and C97-b were used to calibrate the model parameters. The determined parameters (summarized in Table 6) a used to simulate the other four tests.

Table 6 Model parameters for tested soil mixture

Erosion parameters			Filtration parameters		Permeability parameter
λ_e	α_1	α_2	λ_f	β	m_k
151.6	0.89	3.42	170.6	1.0	16

Figure 5 presents the comparison between experimental and numerical results of the erosion. Rochim et al. (2017) characterized the evolution of the cumulative eroded mass with the variation of the cumulative expended energy E_{flow}, computed by the time integration of the instantaneous flow power P_{flow}. Overall, the proposed model was able to reproduce, with reasonable success, the evolution of erosion with different initial fines contents and hydraulic loading histories. However, the predicted results were not totally in agreement with the experimental data for tests A90-a and A90-b. The eroded masses for tests A90-a and A90-b represent only 0.4% (test A90-a) and 1.2% (test A90-b) of their initial fines content, whereas the hydraulic conductivity increased by a factor of 9 (test A90-a) and 4 (test A90-b) at the end of the tests. Obviously, such small loss of mass should not in itself result in such a rapid increase of the hydraulic conductivity. This discrepancy could be explained by the early presence of preferential flows created by particle rearrangements in the case of a lower initial fines content of the soil. In terms of the deviation of the hydraulic conductivity, Ke and Takahashi (2014a, 2014b) attributed it to the difference in homogeneity within the reconstituted soil specimens. Another aspect which has not been taken into account is the unknown influence of the saturation stage, which may also lead to the heterogeneity of the soil sample before erosion. In Yang et al. (2019e), test A90-a was simulated with non-homogenously distributed initial fines content and porosity, it was observed that the clogging at first restricted the water flow, leading to the decrease of the hydraulic conductivity. It could then be blown away, accompanied by a significant increase of the hydraulic conductivity. In Yang et al. (2019c), a random field theory was applied to investigate soil suffusion with a randomly distributed initial porosity (ϕ_0) and

fines content (f_{c0}). It was confirmed that greater variability or lower spatial correlation of ϕ_0 and f_{c0} could facilitate the capture of the fine particles transported by the water flow. More details could be found in Yang et al. (2019e) and Yang et al. (2019c).

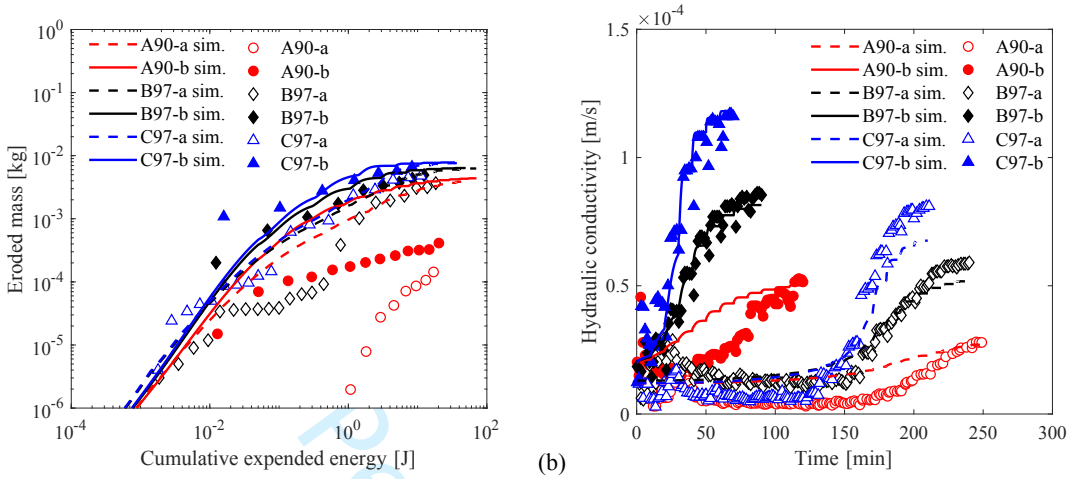

Figure 5 Comparison between laboratory tests (symbols) and simulated data (continuous lines): (a) cumulative eroded masses versus cumulative expended energy; (b) hydraulic conductivity versus time

5. Coupled hydro-mechanical modelling

5.1. Balance of linear momentum

$$\sigma_{ij,i} = w_i \quad \text{.....(14)}$$

$$d\sigma_{ij} = d\sigma'_{ij} + Bdp_w\delta_{ij} = D^{ep}_{ijkl}d\varepsilon_{ij} + Bdp_w\delta_{ij} \quad \text{.....(15)}$$

where σ_{ij} is the component of the total stress tensor, σ'_{ij} is the component of the effective stress tensor, p_w is the pore pressure, B is the Biot effective stress coefficient, δ_{ij} is the Kronecker Delta, w_i is the body force per unit volume. D^{ep}_{ijkl} is the stiffness matrix component of the mechanical model. An f_c-dependent constitutive model (see Table 2 and Eqs.(2) and (3)) was adopted in this study as an example.

5.2. Hydro-mechanical coupling during internal erosion

The hydro-mechanical coupling for internal erosion has been treated as a two-part process. In the first part, the internal erosion leads to an evolution of the porosity and fines content, which in turn leads to the change of the permeability (defined by Eq.(12)). As a consequence, the pore pressure and the effective stresses will change. At the same time, the loss of fine particles due to the seepage flow affects (1) the void ratio and (2) the location of the critical state line, obtained by combining Eqs. (2) and (3) for a sand-silt mixture.

The influence of mechanical process on the hydraulic process, is considered implicitly. The deformation of soil skeleton induced by the mechanical process is considered in the mass balance equations Eqs.(5)-(8) by considering the velocity of the soil skeleton $\mathbf{v}_s$. Therefore, the evolution of ϕ, f_c, c and q_w is the result of combined action of the deformation of soil skeleton ($\mathbf{v}_s$) and the mass exchange between solid-like fine particles and fluidized fine particles ($\hat{n}$). Consequently, the permeability as well as the erosion rate evolves according to Eq. (12) and (13). Moreover, the mass exchange term $\hat{n}$ for the mass balance equations could be formulated to be directly dependent on the stress state according to the experimental results.

5.3. Finite element approach

For the Initial Boundary Value Problem (IBVP) of internal erosion, the following governing equations are formulated:

$$\sigma_{ij,j} - w_j = 0 \quad \text{.....(16)}$$

$$\operatorname{div}(v_s) + \operatorname{div}(q_w) = 0 \quad \text{.....(17)}$$

$$-\frac{\partial(\phi)}{\partial t} + \operatorname{div}(v_s) - \operatorname{div}(\phi v_s) - \hat{n} = 0 \quad \text{.....(18)}$$

$$\frac{\partial(c\phi)}{\partial t} + \operatorname{div}(cq_w) + \operatorname{div}(c\phi v_s) + \hat{n} = 0 \quad \text{.....(19)}$$

$$q_w + \frac{k}{\eta_k \bar{\rho}} \operatorname{grad}(p_w) = 0 \quad \text{.....(20)}$$

It is a system of 5 equations with 5 unknowns $(\mathbf{u}, p_w, \phi, c, \mathbf{q}_w)$ was obtained: the soil skeleton displacement ($\mathbf{u}(\mathbf{x},t)$), the pore pressure ($p_w(\mathbf{x},t)$), the porosity ($\phi(\mathbf{x},t)$), the concentration of fluidized particles ($c(\mathbf{x},t)$) and the flow rate $q_w(\mathbf{x},t)$. For the sake of legibility, the time t and the space $\mathbf{x}$ variables have been omitted in the equations.

This coupled mechanical-erosion process is a non-linear transient problem. Weak forms of the governing partial differential equations were implemented into the finite element code ABAQUS (Hibbitt et al. 2001). ABAQUS provides a user subroutine option (UEL) that allows users to define a new type of element with the user's governing equations and degrees of freedom (DOFs). The global calculate-flow of ABAQUS with the call of UEL subroutine is shown in Figure 6 where the part "**Call UEL**" was developed in this study. In general, Abaqus/UEL solves the overall system of non-linear equations by Newton's method:

$$\mathbf{AMATRX}\cdot\mathbf{d}_N = \mathbf{RHS} \quad \text{.....(21)}$$

where **AMATRX** and **RHS** are the Jacobian matrix and the residual nodal fluxes or forces needed to be defined corresponding to Eqs. (16)-(20); $\mathbf{d}_N$ is the nodal vector of the DOFs $(\mathbf{u}, p_w, \phi, c, \mathbf{q}_w)$. A new isoparametric element has been developed and implemented into ABAQUS via the UEL subroutine. The detailed vector of residual and the Jacobian matrix can be found in Yang et al. (2019a). Note that the systems of governing equations can also be solved by finite difference method.

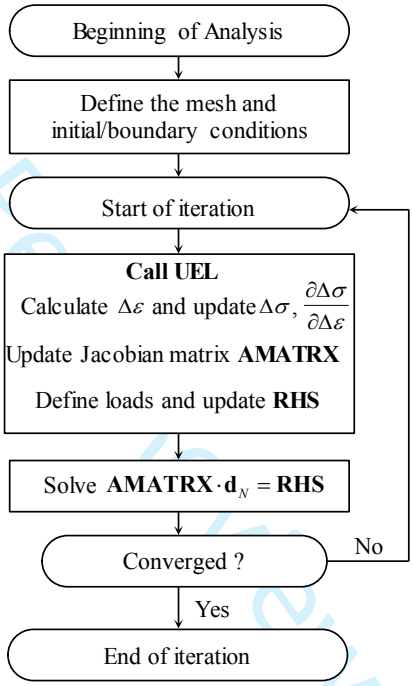

Figure 6 Global calculate-flow chart in ABAQUS with the call of the UEL subroutine

5.4. Performance of the hydro-mechanical model

To illustrate the capacity of the numerical model in treating real scale engineering problems, the developed approach was applied to analyze a typical dike-on-foundation problem. The geometry of this numerical example is shown in Figure 7. The dike was built on an alluvium formation over a limestone bedrock. The dike retains water on the left upstream side, where the water level was located at the top of the dike (*i.e.* 10.5 m), representing an extreme configuration of the flooding condition. The water level at the downstream face was supposed to be located at the bottom of the alluvium layer, below the toe of the dike. The phreatic surface was calculated accordingly (where $p_w = 0kPa$). Above the phreatic surface, the soil is partially saturated. The van Genuchten model (Van Genuchten 1980) was adopted to estimate the relationship between the relative permeability and the degree of water saturation. Furthermore,

it has been reported that, in some cases, karst collapses underneath the foundation might lead to a leakage cavity through which underground water and fine particles could flow out (Gombert et al. 2015). In the simulation, the pore water pressure at the leakage cavity was set to zero. The computations aimed to show how internal erosion may weaken the dike. The alluvium and the dike were considered to be made of the same soil: a mixture of sand and silt. The material parameters (summarized in Table 7, $n_p = n_d = 1$) corresponded to the Ottawa 50/200 sand-silt (Yin et al. 2016) with $e_0 = 0.6$, $c_0 = 0.01$ and $f_{c0} = 0.4$. Due to the lack of experimental data, the filtration was not considered, the ultimate fines content $f_{c,\infty}$ was artificially fixed equal to 0.05, a simple erosion law was adopted (Erosion law ⑥ in Table 5 with λ_e artificially fixed equal to 0.02).

Table 7 Model parameters of Ottawa sand-silt mixture

Elastic parameters			Plastic parameters			CSL-related parameters				Fines parameters			Erosion parameters
G_0/MPa	ν	n	k_p	A_d	ϕ_u	$e_{hc,cr0}$	$e_{fc,cr0}$	ξ	λ	a	m	f_{th}	λ_e
150	0.2	0.5	0.0017	1	32	0.805	1.03	0.196	0.081	0	0.7	0.3	0.02

Only 3 representative results are presented in Figure 8 and Figure 9. Figure 8(a) and Figure 9(a) show the displacement and the deviatoric plastic strain fields within the dike at the end of erosion (time = 30 days). Figure 8(b) show the time evolution the maximum settlement at the top of dike. Figure 9(b) shows the distribution of the fines content at the end of erosion. An area with significant settlement was found at the top of the dike, indicating the inception of a sinkhole as the result of internal erosion. The fine particles close to the leakage cavity were washed out due to high local hydraulic gradients. The sinkhole was formed due to the volumetric settlements induced by a loosened soil matrix. It was noted that an eroded zone also developed near the phreatic surface at the downstream side due to the difference in water pressure at the upstream and downstream faces of the dike. More discussions about the influence of the water level, the size and location of the leakage cavity and the initial value of the fines content could be found in (Yang et al. (2019a); Yang et al. (2020a))

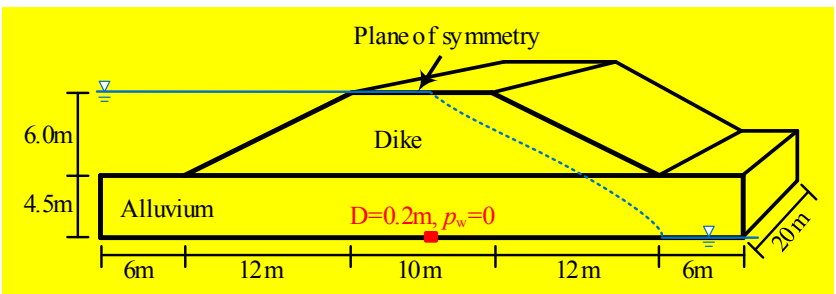

Figure 7 Illustration of the dike-on-foundation with a cavity located at the bottom (1/2 model)

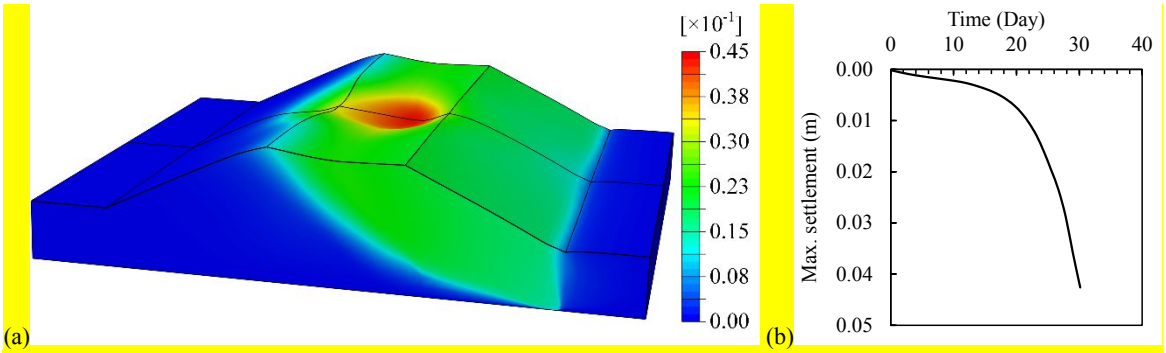

Figure 8 (a) Displacement magnitude field after erosion (Unit: m); (b) Time evolution of the maximum settlement at the top of the dike

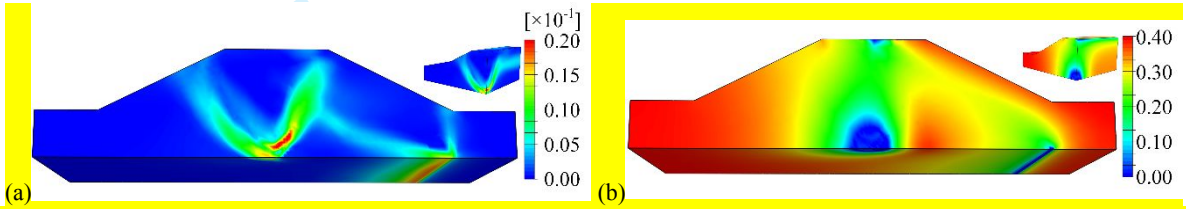

Figure 9 Results of simulation for (a) deviatoric plastic strain field after erosion (1/2 and 1/4 models) and (b) spatial distribution of fines content after erosion (1/2 and 1/4 models)

6. A practical simulation tool for triaxial erosion test

6.1. Model formulation

Under the framework of continuum mechanics, the erosion process is uniform under the assumption of an initially uniform homogeneous specimen. A well-controlled erosion coupled with the mechanical loading triaxial tests on reconstructed specimens can be seen as a case of a representative elementary volume with the hydraulic gradient across the specimen as an input boundary condition. Hence, a simple simulation model for the triaxial tests with internal erosion and mechanical loading can be formulated, which should be useful in evaluating the eroded mass as well as the induced deformation of the soil element.

The hydraulic process of internal erosion could be described by Eqs.(5)-(12), in which the volumetric mass exchange term is given as :

$$\hat{n} = -\lambda_e (1-\phi)(f_c - f_{c\infty})|\mathbf{q}_w| \quad \text{.....(22)}$$

$$f_{c\infty} = f_{c0}\left[\left(1-\frac{\alpha_1}{\exp(\beta\eta/M_p)}\right)\exp\left(-|\mathbf{q}_w|^{\alpha_3}\times 10^{\alpha_2}\right)+\frac{\alpha_1}{\exp(\beta\eta/M_p)}\right] \quad \text{.....(23)}$$

where $f_{c\infty}$ is the ultimate fines content; f_{c0} is the initial fines content; η is the stress ratio; $\alpha_{1\sim3}$, β and λ_e are material parameters. The expression of $f_{c\infty}$ is modified from that proposed by Uzuoka et al. (2012) (shown in Table 5) to account for the influence of stress ratio.

The mechanical behaviors the porous solid is described by an exponential function based incrementally nonlinear constitutive model (Yin et al. 2018). The constitutive equations under axisymmetric triaxial condition are briefly summarized as follows:

$$\delta p' = K\left\{\delta\varepsilon_v - A_d\left(M_{pt} - \frac{q}{p'}\right)\delta\varepsilon_d\left[1-\exp\left(-d\eta\right)\right]\right\} \quad (24)$$

$$\delta q = 3G\delta\varepsilon_d\left(1-\frac{q}{p'M_p}\right)+\frac{q}{p'}\delta p' \quad (25)$$

where the shear and bulk modules G and K, and the stress ratios M_p and M_{pt} are defined in Table 2. $\eta=q/p'$ is defined as the ratio between the deviatoric stress q and the mean effective stress p'; $\delta\varepsilon_d$ and $\delta\varepsilon_v$ are the increment of deviatoric and volumetric strain; the location of CSL is determined by Eq. (3).

6.2. Simulation schemes

During an internal erosion test, the soil specimen is subjected to constant boundary stresses while the amount of eroded fine particles increases progressively. Therefore, the stress ratio η is kept constant while the peak strength ratio M_p and the initial stiffness $G_\eta = 3G/p'$ evolve as a function of the density state of the soil. The shear strain can be incrementally expressed as follows:

$$\delta\varepsilon_d = -\frac{M_p^{(i)}}{G_\eta^{(i)}}\ln\left(1-\frac{\eta^{(i)}}{M_p^{(i)}}\right)+\frac{M_p^{(i-1)}}{G_\eta^{(i-1)}}\ln\left(1-\frac{\eta^{(i-1)}}{M_p^{(i-1)}}\right) \quad (26)$$

with the superscript (i) representing the current loading step and $(i-1)$ the previous loading step. The volumetric strain increment can then be computed as:

$$\delta\varepsilon_v = -\frac{p'}{K^2}\delta K + A_d\left(M_{pt}-\frac{q}{p'}\right)\delta\varepsilon_d\left[1-\exp\left(-d\eta\right)\right] \quad (27)$$

The incremental modification of the void ratio induced by the body deformation is added to the void ratio change caused by erosion:

$$\left(\delta e\right)_{\text{total}} = \left(\delta e\right)_{\text{er}} + \delta\varepsilon_v\left(1+e\right) \quad (28)$$

Under triaxial condition, the axial and radial strain increments ($\delta\varepsilon_a$ and $\delta\varepsilon_r$) are functions of the shear and volumetric strain increments as follows:

$$\delta\varepsilon_a = \delta\varepsilon_d + \frac{1}{3}\delta\varepsilon_v, \quad \delta\varepsilon_r = \frac{1}{3}\delta\varepsilon_v - \frac{1}{2}\delta\varepsilon_d \quad \text{.....(29)}$$

Thus, $\delta\varepsilon_a$ and $\delta\varepsilon_r$ can be used alternatively instead of $\delta\varepsilon_d$ and $\delta\varepsilon_v$.

The numerical modelling scheme can be summarized in Figure 10 for granular media under constant stresses subjected to internal erosion. The set of partial differential equations were solved explicitly in time and by the finite difference method in space, the primary unknowns being $(\mathbf{u}, p_w, \phi, c, f_c)$. Other unknowns, such as the total discharge rate $\mathbf{q}_w$, the density of the mixture $\overline{\rho}$, and the intrinsic permeability k, could be explicitly determined by Eq.(10)-(12).

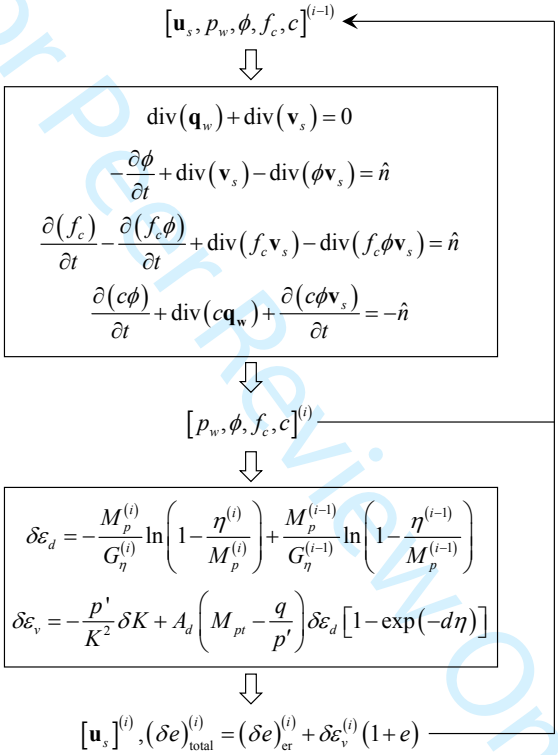

Figure 10 Computation flowchart for internal erosion under constant stresses

In conventional drained triaxial test simulations, the confining stress was maintained constant before and after erosion. Thus, the ratio between the incremental deviatoric stress and the incremental mean effective stress was equal to 3. From Eqs. (24) and (25), the deviatoric stress and the volumetric strain could be obtained by imposing an incremental deviatoric strain as follows:

$$\delta q = 3G\delta\varepsilon_d\left(1-\frac{q}{p'M_p}\right)\Big/\left(1-\frac{q}{3p'}\right) \quad \text{.....(30)}$$

$$\delta p' = \frac{\delta q}{3} \quad \text{.....(31)}$$

$$\delta\varepsilon_v = \frac{\delta p'}{K} + A_d\left(M_{pt} - \frac{q}{p'}\right)\delta\varepsilon_d\left[1-\exp\left(-d\eta\right)\right] \quad \text{.....(32)}$$

Note that the above conventional drained triaxial test simulations were performed on a representative elementary volume, thus the time t and space x were not considered in the simulations. Moreover, the mechanical part could be replaced by any critical state based phenomenological model.

6.3. Performance of the simple practical simulation model

Chang and Zhang (2011) performed several hydraulic-gradient controlled downward erosion tests on gap-graded HK-CDG mixtures under different stress states with a newly developed stress-controlled erosion apparatus. The tested soil was obtained by mixing the commercial washed Leighton Buzzard sand (fraction E) and the completely decomposed granite (CDG) extracted from a construction site on Beacon Hill, Hong Kong. The initial fines content was $f_{c0} = 0.35$.

The tests selected for simulations were summarized in Table 9. BM-C-1, BM-C-2, and BM-C-3 were conventional drained triaxial tests on isotropically consolidated samples without erosion. GS-C-1, GS-C-2, and GS-C-3 were erosion tests under isotropic stress states. GS-C-4, GS-C-5 and GS-C-6 were erosion tests under anisotropic stress states. The hydraulic gradient, i, was increased in stages to the final value (i.e., 0.15 per 10 min for $i \le 1.0$, 0.25 per 10 min for $1.0 < i < 2.0$, and 0.50 per 10 min for $i \ge 2.0$). For 10 min, the hydraulic gradient was increased within the first 2 min and then kept constant for the following 8 min. Once the soil erosion was initiated, the hydraulic gradient was kept constant until no further soil loss was observed (i.e. < 25.0g/m^2 per 10 min). Then, the hydraulic gradient was increased to another level. Drained triaxial tests were carried out on the eroded samples, starting at the stress state applied during the erosion tests.

The elastic parameters (G_0, ν, n), the dilatancy parameters (d, A_d) and the CSL related parameters (λ, ζ) were calibrated basted on a isotropic compression test and three drained triaxial tests (BM-C-1, BM-C-2, and BM-C-3); the erosion parameters (λ_e, α_1, α_2, α_3, m_k) were calibrated by fitting the time evolution of the hydraulic conductivity and the cumulative loss of dry mass in tests GS-C-1 and GS-C-5; due to the lack of data, the values of the other parameters ($e_{hc,cr0}$, $e_{hf,cr0}$, a, m and f_{th}) were assumed based on published data on other similar materials (Yin et al. 2014; Yin et al. 2016). The determined parameters (summarized in

Table 8, $n_p = n_d = 1$) were used to simulate the erosion tests and the drained triaxial tests. Note that a detailed discussion about the parameter calibration using optimization methods is provided in Yang et al. (2020b).

Table 8 Model parameters of HK-CDG mixture

Elastic parameters			Dilatancy parameters		CSL-related parameters					Fines parameters			Erosion parameters				
G_0	ν	n	d	A_d	$e_{hc,cr0}$	$e_{fc,cr0}$	ξ	λ	ϕ_u	a	m	f_{th}	λ_e	α_1	α_2	α_3	m_k
16.7	0.3	0.95	18	0.35	0.8	0.86	0.45	0.03	32	0.79	0.46	0.28	40	0.92	11	3	4

Figure 11 and Figure 12 show the comparison between predicted and experimental results of the erosion tests and the triaxial tests. The proposed numerical approach was able to reproduce the general trend of the soil behaviors up to the peak strength which corresponded in the experiments to the development of strain localization within the specimens. In some cases, discrepancies between experimental and numerical results could be seen, possibly due to the difficulty of measuring accurately certain material properties, such as the elastic stiffness or the friction angle, as a function of the fines content. Another aspect which was not taken into account in the simulations was that heterogeneity within the specimen could be produced by the combined effects of transport and filtration of the fine particles. Not enough detail of this particular aspect was given by Chang (2012). The results demonstrate that the developed model can be practically useful in evaluating the eroded mass, the deformation of the soil during erosion, as well as the degradation of the mechanical properties after erosion.

Table 9 Testing program

Specimen identity	Applied stress state			
	Confining Pressure (kPa)	Effective Mean Stress (kPa)	Deviatoric Stress (kPa)	Stress ratio
①BM-C-1	50	50	0	0
②BM-C-2	100	100	0	0
③BM-C-3	200	200	0	0
④GS-C-1	50	50	0	0
⑤GS-C-2	100	100	0	0
⑥GS-C-3	200	200	0	0
⑦GS-C-4	50	67	50	0.75
⑧GS-C-5	50	83	100	1.2
⑨GS-C-6	50	100	150	1.5

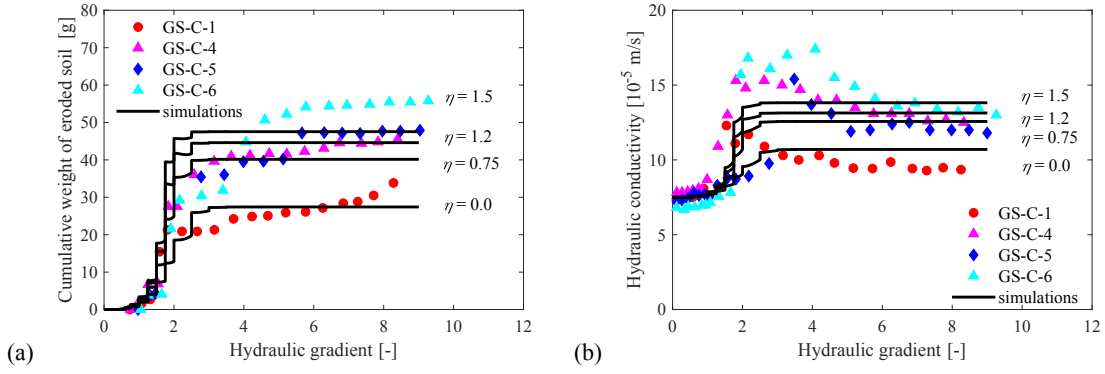

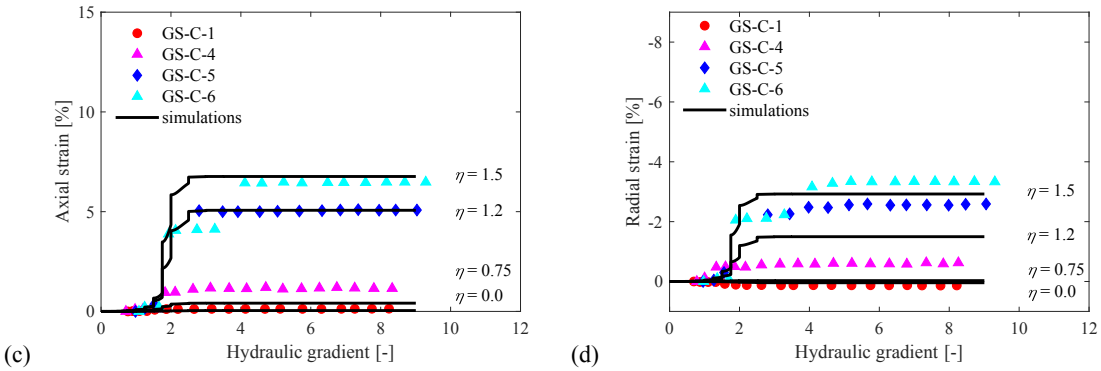

Figure 11 Comparisons between predicted and experimental results of erosion tests (a) Cumulative eroded soil mass; (b) hydraulic conductivity; (c) axial strain and (d) radial strain

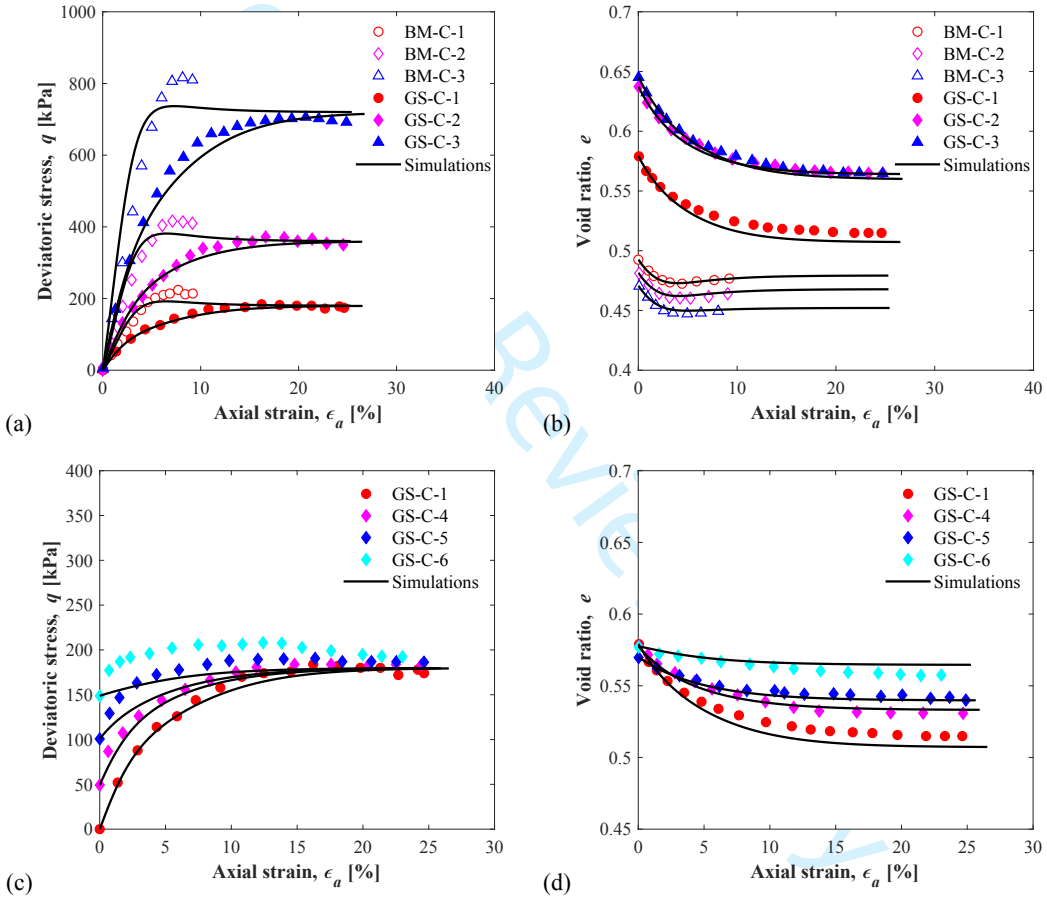

Figure 12 Comparisons between predicted and experimental results of triaxial tests (a,c) deviatoric stress versus axial strain and (b,d) void ratio versus axial strain. Hollow points indicate triaxial compression of the initial specimen, and solid points indicate triaxial compression of eroded samples.

7. Conclusion

In this paper, the hydro-mechanical continuous modelling of granular soils considering suffusion was systematically reviewed. One of the necessary features in constitutive modelling of soil behaviors is the critical state concept with an interlocking effect. A unified formulation was adopted to determine the position of the critical state line of sand-silt mixtures as a function

of the fines content. Then, based on the porous medium theory, a four-constituent numerical model was adopted to describe the internal erosion. The model consisted of modelling the erosion of the soil skeleton, the transport by the water flow and the filtration of the fine particles through the mass exchange between the solid and fluid phases. The terms of mass exchange were introduced into the mass balance equations complemented by a filtration term in order to simulate the filling of the initial voids due to the filtration of the transported fines from the suspension to the solid fraction.

In order to perform analyses at the scale of an entire engineering structure, a more general elastoplastic sand-silt mixture model was introduced within the four-constituent model of suffusion. The hydro-mechanical model was first implemented into the commercial finite element code ABAQUS and used to assess how internal erosion could impact the stability of earthen structures. Meanwhile, a simple simulation model for the triaxial tests with internal erosion and mechanical loading was developed. The four-constituent model was enhanced by including an exponential function based incrementally nonlinear constitutive model to account for the effects of the evolution of the fines content on the behaviors of the soil. A practical numerical platform was then developed to simulate the downward erosion tests under triaxial mechanical loading with a special emphasis on the evolution of the eroded mass, the hydraulic conductivity and the deformation of the specimen during and after erosion.

The performance of the numerical model was verified by simulating laboratory tests as well as an example of the dike-on-foundation problem. For each component of the model (mechanical model, f_c-dependency and erosion law), alternative choices can be made.

These results should provide some inspiration for the design of future experiments and improve the understanding of the origin of damages or failures induced by internal erosion within earthen structures. They should also serve as a reference to update the specifications for design, construction, and adaptation in order to mitigate and prevent the highest risks.

Acknowledgement

The financial supports provided by the Research Grants Council (RGC) of Hong Kong Special Administrative Region Government (HKSARG) of China (Grant No.: 15209119, PolyU R5037-18F) and the National Institute for Industrial Environment and Risks of France (INERIS) are gratefully acknowledged.

References

Bonelli, S., and Marot, D. On the modelling of internal soil erosion. *In* The 12th International Conference of International Association for Computer Methods and Advances in Geomechanics (IACMAG). 2008. p. 7.

Chang, C., and Hicher, P.-Y. 2005. An elasto-plastic model for granular materials with microstructural consideration. International Journal of Solids and Structures, **42**(14): 4258-4277.

Chang, C.S., and Yin, Z.-Y. 2009. Micromechanical modeling for inherent anisotropy in granular materials. Journal of engineering mechanics, **136**(7): 830-839.

Chang, C.S., and Yin, Z.-Y. 2011. Micromechanical modeling for behavior of silty sand with influence of fine content. International Journal of Solids and Structures, **48**(19): 2655-2667.

Chang, C.S., and Deng, Y. 2018. A nonlinear packing model for multi-sized particle mixtures. Powder technology, **336**: 449-464.

Chang, D., and Zhang, L. 2011. A stress-controlled erosion apparatus for studying internal erosion in soils. Geotechnical Testing Journal., **34**(6): 579-589.

Cividini, A., and Gioda, G. 2004. Finite-element approach to the erosion and transport of fine particles in granular soils. International Journal of Geomechanics, **4**(3): 191-198.

Cividini, A., Bonomi, S., Vignati, G.C., and Gioda, G. 2009. Seepage-induced erosion in granular soil and consequent settlements. International Journal of Geomechanics, **9**(4): 187-194.

Crosta, G., and Prisco, C.d. 1999. On slope instability induced by seepage erosion. Canadian Geotechnical Journal, **36**(6): 1056-1073.

Darve, F. 1990. The expression of rheological laws in incremental form and the main classes of constitutive equations. *In* Geomaterials: Constitutive Equations and Modelling. CRC Press. pp. 139-164.

Darve, F., and Labanieh, S. 1982. Incremental constitutive law for sands and clays: simulations of monotonic and cyclic tests. International Journal for Numerical and Analytical Methods in Geomechanics, **6**(2): 243-275.

de Boer, R. 2000. Contemporary progress in porous media theory. Applied Mechanics Reviews, **53**(12): 323-370.

Duncan, J.M., and Chang, C.-Y. 1970. Nonlinear analysis of stress and strain in soils. Journal of Soil Mechanics & Foundations Div.

Fell, R., Wan, C.F., Cyganiewicz, J., and Foster, M. 2003. Time for development of internal erosion and piping in embankment dams. Journal of geotechnical and geoenvironmental engineering, **129**(4): 307-314.

Gajo, A., and Wood, M. 1999. Severn–Trent sand: a kinematic-hardening constitutive model: the q–p formulation. Geotechnique, **49**(5): 595-614.

Gombert, P., Orsat, J., Mathon, D., Alboresha, R., Al Heib, M., and Deck, O. 2015. Role des effondrements karstiques sur les desordres survenus sur les digues de Loire dans le Val D'Orleans (France). Bulletin of Engineering Geology and the Environment, **74**(1): 125-140.

Hibbitt, Karlsson, and Sorensen. 2001. ABAQUS/standard User's Manual. Hibbitt, Karlsson & Sorensen.

Hicher, P.-Y. 2013. Modelling the impact of particle removal on granular material behaviour. Géotechnique, **63**(2): 118.

Hosn, R.A., Sibille, L., Benahmed, N., and Chareyre, B. 2018. A discrete numerical model involving partial fluid-solid coupling to describe suffusion effects in soils. Computers and Geotechnics, **95**: 30-39.

Hu, W., Hicher, P.-Y., Scaringi, G., Xu, Q., Van Asch, T., and Wang, G. 2018. Seismic precursor to instability induced by internal erosion in loose granular slopes. Géotechnique: 1-13.

Jefferies, M. 1993. Nor-Sand: a simle critical state model for sand. Géotechnique, **43**(1): 91-103.

Jin, Y.-F., Yin, Z.-Y., Shen, S.-L., and Hicher, P.-Y. 2016. Selection of sand models and identification of parameters using an enhanced genetic algorithm. International Journal for Numerical and Analytical Methods in Geomechanics, **40**(8): 1219-1240. doi:10.1002/nag.2487.

Jin, Y.-F., Wu, Z.-X., Yin, Z.-Y., and Shen, J.S. 2017. Estimation of critical state-related formula in advanced constitutive modeling of granular material. Acta Geotechnica, **12**(6): 1329-1351.

Jin, Y.-F., Yin, Z.-Y., Wu, Z.-X., and Zhou, W.-H. 2018. Identifying parameters of easily crushable sand and application to offshore pile driving. Ocean Engineering, **154**: 416-429. doi:10.1016/j.oceaneng.2018.01.023.

Ke, L., and Takahashi, A. 2014a. Triaxial erosion test for evaluation of mechanical consequences of internal erosion. Geotechnical Testing Journal, **37**(2): 347-364.

Ke, L., and Takahashi, A. 2014b. Experimental investigations on suffusion characteristics and its mechanical consequences on saturated cohesionless soil. Soils and Foundations, **54**(4): 713-730.

Kenney, T., and Lau, D. 1985. Internal stability of granular filters. Canadian Geotechnical Journal, **22**(2): 215-225.

Khalil, T., Saiyouri, N., Muresan, B., and Hicher, P.Y. 2013. Internal erosion of chemically reinforced granular materials: a mathematical modeling approach. International Journal for Numerical and Analytical Methods in Geomechanics, **37**(5): 491-502.

Kolymbas, D. 1991. An outline of hypoplasticity. Archive of applied mechanics, **61**(3): 143-151.

Li, X.-S., and Wang, Y. 1998. Linear representation of steady-state line for sand. Journal of geotechnical and geoenvironmental engineering, **124**(12): 1215-1217.

Liu, X., Qu, S., and Huang, J. 2019. Relationship between physical properties and particle-size distribution of geomaterials. Construction and Building Materials, **222**: 312-318.

Liu, X., Qu, S., Chen, R., and Chen, S. 2018. Development of a Two-Dimensional Fractal Model for Analyzing the Particle Size Distribution of Geomaterials. Journal of Materials in Civil Engineering, **30**(8): 04018175.

Lominé, F., Scholtès, L., Sibille, L., and Poullain, P. 2013. Modeling of fluid–solid interaction in granular media with coupled lattice Boltzmann/discrete element methods:

application to piping erosion. International Journal for Numerical and Analytical Methods in Geomechanics, **37**(6): 577-596.

Mansouri, M., El Youssoufi, M.S., and Nicot, F. 2017. Numerical simulation of the quicksand phenomenon by a 3D coupled Discrete Element-Lattice Boltzmann hydromechanical model. International Journal for Numerical and Analytical Methods in Geomechanics, **41**(3): 338-358.

Mašín, D. 2005. A hypoplastic constitutive model for clays. International Journal for Numerical and Analytical Methods in Geomechanics, **29**(4): 311-336.

Mašín, D., and Khalili, N. 2012. A thermo-mechanical model for variably saturated soils based on hypoplasticity. International Journal for Numerical and Analytical Methods in Geomechanics, **36**(12): 1461-1485.

Minh, N., and Cheng, Y. 2013. A DEM investigation of the effect of particle-size distribution on one-dimensional compression. Géotechnique, **63**(1): 44-53.

Miura, N., Murata, H., and Yasufuku, N. 1984. Stress-strain characteristics of sand in a particle-crushing region. Soils and Foundations, **24**(1): 77-89.

Muir Wood, D. 2007. The magic of sands—the 20th Bjerrum Lecture presented in Oslo, 25 November 2005. Canadian Geotechnical Journal, **44**(11): 1329-1350.

Muir Wood, D., Maeda, K., and Nukudani, E. 2010. Modelling mechanical consequences of erosion. Géotechnique, **60**(6): 447-457.

Nicot, F., and Darve, F. 2011. The H-microdirectional model: accounting for a mesoscopic scale. Mechanics of Materials, **43**(12): 918-929.

Niemunis, A., and Herle, I. 1997. Hypoplastic model for cohesionless soils with elastic strain range. Mechanics of Cohesive-frictional Materials: An International Journal on Experiments, Modelling and Computation of Materials and Structures, **2**(4): 279-299.

Papadopoulou, A., and Tika, T. 2008. THE EFFECT OF FINES ON CRITICAL STATE AND LIQUEFACTION RESISTANCE CHARACTERISTICS OF NON-PLASTIC SILTY SANDS. Soils and Foundations, **48**(5): 713-725. doi:10.3208/sandf.48.713.

Papamichos, E., Vardoulakis, I., Tronvoll, J., and Skjaerstein, A. 2001. Volumetric sand production model and experiment. International Journal for Numerical and Analytical Methods in Geomechanics, **25**(8): 789-808.

Reboul, N., Vincens, E., and Cambou, B. 2008. A statistical analysis of void size distribution in a simulated narrowly graded packing of spheres. Granular Matter, **10**(6): 457-468.

Reddi, L.N., Lee, I.-M., and Bonala, M.V. 2000. Comparison of internal and surface erosion using flow pump tests on a sand-kaolinite mixture. Geotechnical Testing Journal, **23**(1): 116-122.

Revil, A., and Cathles, L. 1999. Permeability of shaly sands. Water Resources Research, **35**(3): 651-662.

Rochim, A., Marot, D., Sibille, L., and Thao Le, V. 2017. Effects of Hydraulic Loading History on Suffusion Susceptibility of Cohesionless Soils. Journal of geotechnical and geoenvironmental engineering, **143**(7): 04017025.

Rönnqvist, H., Fannin, J., and Viklander, P. 2014. On the use of empirical methods for assessment of filters in embankment dams. Géotechnique Letters, **4**(4): 272-282.

Sari, H., Chareyre, B., Catalano, E., Philippe, P., and Vincens, E. Investigation of internal erosion processes using a coupled dem-fluid method. *In* Particles 2011 II International Conference on Particle-Based Methods, E. Oate and DRJ Owen (Eds), Barcelona. 2011. pp. 1-11.

Schaufler, A., Becker, C., and Steeb, H. 2013. Infiltration processes in cohesionless soils. ZAMM-Journal of Applied Mathematics and Mechanics/Zeitschrift für Angewandte Mathematik und Mechanik, **93**(2-3): 138-146.

Scholtès, L., Hicher, P.-Y., and Sibille, L. 2010. Multiscale approaches to describe mechanical responses induced by particle removal in granular materials. Comptes Rendus Mécanique, **338**(10-11): 627-638.

Shen, C., Liu, S., Xu, S., and Wang, L. 2019. Rapid estimation of maximum and minimum void ratios of granular soils. Acta Geotechnica, **14**(4): 991-1001.

Sibille, L., Lominé, F., Poullain, P., Sail, Y., and Marot, D. 2015. Internal erosion in granular media: direct numerical simulations and energy interpretation. Hydrological Processes, **29**(9): 2149-2163.

Stavropoulou, M., Papanastasiou, P., and Vardoulakis, I. 1998. Coupled wellbore erosion and stability analysis. International Journal for Numerical and Analytical Methods in Geomechanics, **22**(9): 749-769.

Steeb, H., and Diebels, S. 2003. A thermodynamic-consistent model describing growth and remodeling phenomena. Computational materials science, **28**(3): 597-607.

Steeb, H., Diebels, S., and Vardoulakis, I. 2007. Modeling internal erosion in porous media. *In* Computer Applications In Geotechnical Engineering. pp. 1-10.

Sterpi, D. 2003. Effects of the erosion and transport of fine particles due to seepage flow. international journal of Geomechanics, **3**(1): 111-122.

Taiebat, M., and Dafalias, Y.F. 2008. SANISAND: Simple anisotropic sand plasticity model. International Journal for Numerical and Analytical Methods in Geomechanics, **32**(8): 915-948.

Thevanayagam, S., Shenthan, T., Mohan, S., and Liang, J. 2002. Undrained Fragility of Clean Sands, Silty Sands, and Sandy Silts. Journal of geotechnical and geoenvironmental engineering, **128**(10): 849-859. doi:doi:10.1061/(ASCE)1090-0241(2002)128:10(849).

Uzuoka, R., and Borja, R.I. 2012. Dynamics of unsaturated poroelastic solids at finite strain. International Journal for Numerical and Analytical Methods in Geomechanics, **36**(13): 1535-1573.

Uzuoka, R., Ichiyama, T., Mori, T., and Kazama, M. Hydro-mechanical analysis of internal erosion with mass exchange between solid and water. *In* 6th International Conference on Scour and Erosion. 2012. pp. 655-662.

Van Genuchten, M.T. 1980. A closed-form equation for predicting the hydraulic conductivity of unsaturated soils. Soil science society of America journal, **44**(5): 892-898.

Vardoulakis, I., Stavropoulou, M., and Papanastasiou, P. 1996. Hydro-mechanical aspects of the sand production problem. Transport in porous media, **22**(2): 225-244.

Vermeer, P. 1978. A double hardening model for sand. Géotechnique, **28**(4): 413-433.

Wan, C.F., and Fell, R. 2004. Investigation of rate of erosion of soils in embankment dams. Journal of geotechnical and geoenvironmental engineering, **130**(4): 373-380.

Wan, R., and Pouragha, M. 2015. Fabric and connectivity as field descriptors for deformations in granular media. Continuum Mechanics and Thermodynamics, **27**(1-2): 243-259.

Wan, R.G., and Guo, P.J. 1998. A simple constitutive model for granular soils: Modified stress-dilatancy approach. Computers and Geotechnics, **22**(2): 109-133. doi:https://doi.org/10.1016/S0266-352X(98)00004-4.

Wu, W., and Kolymbas, D. 2000. Hypoplasticity then and now. Constitutive modelling of granular materials: 57-105.

Wu, W., Bauer, E., and Kolymbas, D. 1996. Hypoplastic constitutive model with critical state for granular materials. Mechanics of Materials, **23**(1): 45-69.

Wu, Z.-X., Yin, Z.-Y., Jin, Y.-F., and Geng, X.-Y. 2017. A straightforward procedure of parameters determination for sand: a bridge from critical state based constitutive modelling to finite element analysis. European Journal of Environmental and Civil Engineering: 1-23.

Wu, Z.-X., Yin, Z.-Y., Jin, Y.-F., and Geng, X.-Y. 2019. A straightforward procedure of parameters determination for sand: a bridge from critical state based constitutive modelling to finite element analysis. European Journal of Environmental and Civil Engineering, **23**(12): 1444-1466. doi:10.1080/19648189.2017.1353442.

Xu, Y., and Zhang, L. 2009. Breaching parameters for earth and rockfill dams. Journal of geotechnical and geoenvironmental engineering, **135**(12): 1957-1970.

Yang, J., Yin, Z.Y., Laouafa, F., and Hicher, P.Y. 2019a. Internal erosion in dike-on-foundation modeled by a coupled hydromechanical approach. International Journal for Numerical and Analytical Methods in Geomechanics, **43**(3): 663-683.

Yang, J., Yin, Z.-Y., Laouafa, F., and Hicher, P.-Y. 2019b. Hydromechanical modeling of granular soils considering internal erosion. Canadian Geotechnical Journal, **57**(2): 157-172. doi:10.1139/cgj-2018-0653.

Yang, J., Yin, Z.-Y., Laouafa, F., and Hicher, P.-Y. 2019c. Analysis of suffusion in cohesionless soils with randomly distributed porosity and fines content. Computers and Geotechnics, **111**: 157-171. doi:https://doi.org/10.1016/j.compgeo.2019.03.011.

Yang, J., Yin, Z.-Y., Laouafa, F., and Hicher, P.-Y. 2019d. Hydro-mechanical modeling of granular soils considering internal erosion. Canadian Geotechnical Journal. doi:10.1139/cgj-2018-0653.

Yang, J., Yin, Z.-Y., Laouafa, F., and Hicher, P.-Y. 2019e. Modeling coupled erosion and filtration of fine particles in granular media. Acta Geotechnica, **14**(6): 1615-1627. doi:10.1007/s11440-019-00808-8.

Yang, J., Yin, Z.-Y., Laouafa, F., and Hicher, P.-Y. 2020a. Three-dimensional hydromechanical modeling of internal erosion in dike-on-foundation. International Journal for Numerical and Analytical Methods in Geomechanics, **44**(8): 1200-1218. doi:10.1002/nag.3057.

Yang, J., Jin, Y.-F., Yin, Z.-Y., Laouafa, F., and Hicher, P.-Y. 2020b. Identifying the parameters of a hydro-mechanical model for internal erosion occurring in granular soils by using an enhanced backtracking search algorithm. European Journal of Environmental and Civil Engineering: 1-20. doi:10.1080/19648189.2020.1752809.

Yang, S.L., Sandven, R., and Grande, L. 2006. Instability of sand–silt mixtures. Soil Dynamics and Earthquake Engineering, **26**(2): 183-190. doi:https://doi.org/10.1016/j.soildyn.2004.11.027.

Yao, Y.-P., Kong, L.-M., Zhou, A.-N., and Yin, J.-H. 2014. Time-dependent unified hardening model: three-dimensional elastoviscoplastic constitutive model for clays. Journal of engineering mechanics, **141**(6): 04014162.

Yao, Y., Sun, D., and Luo, T. 2004. A critical state model for sands dependent on stress and density. International Journal for Numerical and Analytical Methods in Geomechanics, **28**(4): 323-337.

Yao, Y., Sun, D., and Matsuoka, H. 2008. A unified constitutive model for both clay and sand with hardening parameter independent on stress path. Computers and Geotechnics, **35**(2): 210-222.

Yao, Y., Hou, W., and Zhou, A. 2009. UH model: three-dimensional unified hardening model for overconsolidated clays. Geotechnique, **59**(5): 451-469.

Yin, Z.-Y., Chang, C.S., and Hicher, P.-Y. 2010. Micromechanical modelling for effect of inherent anisotropy on cyclic behaviour of sand. International Journal of Solids and Structures, **47**(14-15): 1933-1951.

Yin, Z.-Y., Zhao, J., and Hicher, P.-Y. 2014. A micromechanics-based model for sand-silt mixtures. International Journal of Solids and Structures, **51**(6): 1350-1363.

Yin, Z.-Y., Huang, H.-W., and Hicher, P.-Y. 2016. Elastoplastic modeling of sand–silt mixtures. Soils and Foundations, **56**(3): 520-532.

Yin, Z.-Y., Wu, Z.-X., and Hicher, P.-Y. 2018. Modeling Monotonic and Cyclic Behavior of Granular Materials by Exponential Constitutive Function. Journal of engineering mechanics, **144**(4): 04018014.

Yu, A., and Standish, N. 1987. Porosity calculations of multi-component mixtures of spherical particles. Powder technology, **52**(3): 233-241.

Yu, A., and Standish, N. 1988. An analytical—parametric theory of the random packing of particles. Powder technology, **55**(3): 171-186.

Yu, H. 1998. CASM: A unified state parameter model for clay and sand. International Journal for Numerical and Analytical Methods in Geomechanics, **22**(8): 621-653.

Zhang, F., Li, M., Peng, M., Chen, C., and Zhang, L. 2018. Three-dimensional DEM modeling of the stress–strain behavior for the gap-graded soils subjected to internal erosion. Acta Geotechnica: 1-17.

Zhang, L., and Chen, Q. 2006. Seepage failure mechanism of the Gouhou rockfill dam during reservoir water infiltration. Soils and Foundations, **46**(5): 557-568.

Zhang, L., Xu, Y., and Jia, J. 2009. Analysis of earth dam failures: A database approach. Georisk, **3**(3): 184-189.

Zhang, X., Wong, H., Leo, C., Bui, T., Wang, J., Sun, W., and Huang, Z. 2013. A thermodynamics-based model on the internal erosion of earth structures. Geotechnical and Geological Engineering, **31**(2): 479-492.

Zhao, J., and Shan, T. 2013. Coupled CFD–DEM simulation of fluid–particle interaction in geomechanics. Powder technology, **239**: 248-258.

Zlatović, S., and Ishihara, K. On the influence of nonplastic fines on residual strength. *In* First International Conference on Earthquake Geotechnical Engineering. 1995. pp. 239-244.

Figure captions

Figure 1 Comparison between experiments and simulations for drained (a-b) and undrained triaxial tests (c-d) on Toyoura sand: (a,c) deviatoric stress versus axial strain, (b) void ratio versus axial strain

Figure 2 (a) Initial void ratios and initial critical void ratios and (b) initial density state (*e0*/*ec*) of selected tests

Figure 3 Comparison of experimental results and simulations for Foundry sand subjected to undrained triaxial tests, with fines content varying from 0 to 100%

Figure 4 REV of a fully-saturated soil mixture and the four-constituent continuum model

Figure 5 Comparison between laboratory tests (symbols) and simulated data (continuous lines): (a) cumulative eroded masses versus cumulative expended energy; (b) hydraulic conductivity

Figure 6 Global calculate-flow chart in ABAQUS with the call of the UEL subroutine

Figure 7 Illustration of the dike-on-foundation with a cavity located at the bottom

Figure 8 (a) Displacement magnitude field after erosion (Unit: m)

Figure 9 Results of simulation for spatial distribution of fines content after erosion (1/2 and 1/4 models)

Figure 10 Computation flowchart for internal erosion under constant stresses

Figure 11 Comparisons between predicted and experimental results of erosion tests (a) Cumulative eroded soil mass; (b) hydraulic conductivity; (c) axial strain and (d) radial strain

Figure 12 Comparisons between predicted and experimental results of triaxial tests (a,c) deviatoric stress versus axial strain and (b,d) void ratio versus axial strain. Hollow points indicate triaxial compression of the initial specimen, and solid points indicate triaxial compression of eroded samples.